

Marquette University

e-Publications@Marquette

Chemistry Faculty Research and Publications

Chemistry, Department of

2-2019

Proton-Coupled Reduction of An Iron Nitrosyl Porphyrin in The Protic Ionic Liquid Nanodomain

Abderrahman Atifi
Marquette University

Piotr J. Mak
Marquette University, piotr.mak@marquette.edu

Michael D. Ryan
Marquette University, michael.ryan@marquette.edu

Follow this and additional works at: https://epublications.marquette.edu/chem_fac

 Part of the [Chemistry Commons](#)

Recommended Citation

Atifi, Abderrahman; Mak, Piotr J.; and Ryan, Michael D., "Proton-Coupled Reduction of An Iron Nitrosyl Porphyrin in The Protic Ionic Liquid Nanodomain" (2019). *Chemistry Faculty Research and Publications*. 998.

https://epublications.marquette.edu/chem_fac/998

Marquette University

e-Publications@Marquette

Chemistry Faculty Research and Publications/College of Arts and Sciences

This paper is NOT THE PUBLISHED VERSION; but the author's final, peer-reviewed manuscript. The published version may be accessed by following the link in the citation below.

Electrochimica Acta, Vol. 295 (February 2019): 735-741. [DOI](#). This article is © Elsevier and permission has been granted for this version to appear in [e-Publications@Marquette](#). Elsevier does not grant permission for this article to be further copied/distributed or hosted elsewhere without the express permission from Elsevier

Proton-Coupled Reduction of An Iron Nitrosyl Porphyrin in The Protic Ionic Liquid Nanodomain

Abderrahman Atifi

Chemistry Department, Marquette University, Milwaukee, WI

Piotr J. Mak

Chemistry Department, Marquette University, Milwaukee, WI

Michael D. Ryan

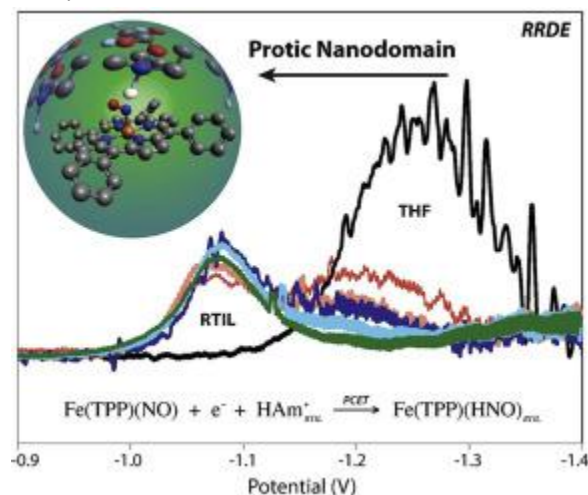
Chemistry Department, Marquette University, Milwaukee, WI

Abstract

The one-electron reduction of many molecules becomes much more favorable if combined with proton transfers or strong hydrogen bonding. Protic room temperature ionic liquids (RTILs), which can form nanodomains in solutions with molecular solvents (MS), can provide an efficient avenue for this process. In this work, we report on the voltammetry, UV/visible and resonance Raman spectroelectrochemistry of Fe(TPP)(NO) in the presence of aprotic/protic ammonium-based ionic liquids. While aprotic RTILs did shift the reduction to more positive potentials, similar shifts could be observed at much lower concentrations of

diethylmethylammonium triflate (HAmOTf, a protic ionic liquid). Deconvolution of the rotating ring-disk electrode (RRDE) voltammetry revealed the partitioning of the reduced species into the ionic liquid nanodomains at low concentrations. The potential shift was substantially in excess of the value expected based on the pK_a of the weak acid. Upon the addition of small amounts of the protic RTIL, the electrochemically or chemically generated anion, $\text{Fe}(\text{TPP})(\text{NO})^-$, reacted rapidly with the HAm^+ acid, forming a $\text{Fe}(\text{TPP})(\text{HNO})$ complex. Further reduction to $\text{Fe}(\text{TPP})(\text{NH}_2\text{OH})$ could be observed on the spectroelectrochemical time scale. The outcome of this work revealed the advantageous role of protic RTIL nanodomains in accelerating the proton-coupled reductions to form more energetically favorable product.

Graphical abstract



Keywords

Rotating ring disk voltammetry, Spectroelectrochemistry, RTIL, Iron porphyrin nitrosyl, Resonance Raman spectroscopy

1. Introduction

The $\text{Fe}(\text{HNO})$ intermediate, formed by protonation of the initial reduction product, iron-nitrosyl, has been postulated as an intermediate in a number of enzymes (cytochrome c nitrite reductases (ccNiR) [1,2], fungal cytochrome P450 nitric oxide reductase (P450nor) [3,4], and hydroxylamine oxidoreductase [5]). The formation and reactions of metalloporphyrin HNO complexes have been reviewed by Doctorovich et al. [6]. A detailed QM/MM study of P450nor was carried out by Riplinger and Neese [7] showing a Fe-HNO intermediate was formed prior to the generation of N_2O . Bylov and Neese [2] also carried out DFT calculations on ccNiR, and found that the HNO complex was an important intermediate on the reduction of nitrite to ammonia. Similar intermediates were found for hydroxylamine oxidoreductase by Attia and Silaghi-Dumitrescu [8], which carries out the reverse of the ccNiR (ammonia to nitrite) reaction.

In order to observe and understand these unstable intermediates, as well as characterizing their spectroscopic features and chemical reactivity, model studies of Fe-HNO complexes have been carried out. Abucayon et al. [9] reported a $\text{Fe}(\text{OEP})(\text{HNO})(\text{Im})$ (OEP = octaethylporphyrin; Im = imidazole) complex that was formed by the reduction of the ferric nitrosyl species with a hydride reducing agent. Goodrich et al. [10] described the formation of an Fe-HNO complex using a picket fence porphyrin.

The spectroelectrochemistry and voltammetry of $\text{Fe}(\text{OEP})(\text{NO})$ in the presence of weak acids also led to the formation of a $\text{Fe}(\text{OEP})(\text{HNO})$ complex which was characterized by visible and NMR spectroscopy [11]. In this study, it was found that the visible spectra of $\text{Fe}(\text{OEP})(\text{NO})$ and $\text{Fe}(\text{OEP})(\text{HNO})$ were quite similar, and, in the

presence of excess acid, the Fe(OEP)(HNO) complex could be further reduced to Fe(OEP)(H₂NOH). Both the Fe(OEP)(HNO) and Fe(OEP)(H₂NOH) species can be slowly oxidized back to the starting Fe(OEP)(NO) complex.

The formation of protonated intermediates is not limited to NO. Other small molecules such as CO₂ need to avoid the formation of the high energy radical anionic species for efficient reduction. For example, the catalytic reduction of CO₂ has been shown to be accelerated by the presence of room temperature ionic liquids (RTIL) [12]. The key step in most of these catalyses is the protonation of the intermediate, which lowers the energy for further reduction by removing the coulombic repulsion towards the addition of additional electrons. The use of protic/aprotic ionic liquids has been shown to alter the thermodynamics and the outcome of the reduction product of CO₂ activation [13]. Previous work on voltammetry in RTILs has shown significant shifts in redox potential in RTILs due to ion pairing between the electrogenerated ion and the RTIL. For example, the two one-electron reduction of 1,4-dinitrobenzene collapses to a single two-electron reduction in RTILs [14,15]. However advantageous RTILs are, they have significant drawbacks due to their high viscosity and cost. Both these disadvantages can be minimized by using mixed RTIL/molecular solvents (MS).

Ionic liquids generally contain large organic cations and small anions, which do not form solids due to weakened coulombic attractions. RTILs can be considered as structured, nanosegregated liquids [16,17]. There are four recognized regimes in RTIL/MS mixtures, depending upon the ratio of RTIL to MS [18]. When the concentration of the RTIL is low, the ions dissociate as a simple electrolyte [19]. At higher concentrations of RTIL, aggregates (nanodomains) form [18]. Molecular dynamics shows that the RTIL nanodomains in RTIL/MS mixtures have a filamentous structure along with isolated ions [16]. Simulation of acetonitrile/RTIL mixtures showed the formation of aggregates at relatively low mole fractions of the RTIL [16]. In RTIL-rich mixtures, the MS will be a dilute solute, interacting with the RTIL domain [18]. The fourth regime is the neat RTIL.

Vaz et al. [20] found experimental evidence of nanostructuration using alcohols as a probe of the RTIL structure in mixtures. Scharf et al. [21] studied ion pairing and the dynamics of the RTIL in chloroform mixtures using NMR. They observed a progression from ion pairs to aggregate formation as the RTIL concentration increased. Tubbs and Hoffmann [22] found evidence for MS and RTIL nanodomains using proton NMR. The presence of MS and RTIL nanodomains were also observed in infrared spectroscopy which showed two different vibrations for the carbonyl group of Ni(OEPone)⁻ (OEPone = octaethylporphyrinone) [23]. The lower energy band interacted strongly with the RTIL nanodomain, while the higher energy carbonyl band was in the MS nanodomain. Similarly, strong ion pairing interactions between RTIL nanodomains and C₆₀²⁻ or C₆₀³⁻ ions have been observed [24]. These results were consistent with a RTIL nanodomain rather than simply ion pairing in the molecular solvent. These nanodomains can lead to additional stabilization of the electrogenerated species [14,[23], [24], [25]].

The interactions between the substrate and the RTIL nanodomains in the work above were primarily electrostatic. Protic RTILs though have the advantage of forming hydrogen bonds or covalent bonds by the transfer of the proton from the RTIL cation to the substrate. These interactions should be much stronger than a purely electrostatic effect, and lead to substrate reductions at more positive potentials. To investigate this, the reaction of Fe(TPP)(NO)⁻, a model of a key intermediate in the enzymatic nitrogen cycle, will be studied using a protic RTIL media. Limited work has been done so far on the reactivity of iron porphyrin nitrosyl complexes in the presence of RTILs [26]. The formation of RTIL nanodomains should be quite advantageous by accelerating the protonation reaction, which will drive the formation of a neutral, and more energetically favorable protonated product.

2. Experimental

2.1. Chemicals

Tetrabutylammonium perchlorate (TBAP), iron(III) tetraphenyl porphyrin (Fe(TPP)(Cl)), hydroxylamine-^{14/15}N hydrochloride (98%), tetrabutylammonium borohydride (98%), and ethyldimethylpropylammonium bis(trifluoromethylsulfonyl)imide (EDPAmNTf₂) were purchased from Sigma-Aldrich Chemical Co. Diethylmethylammonium triflate (HAmOTf, 98%) was purchased from IoLiTec Inc. TBAP was dried at 90 °C under a vacuum overnight before use. Anhydrous THF was refluxed in the presence of sodium metal and benzophenone until the solution was a persistent dark blue color. After purification, the solvent was collected under argon and stored in the glovebox. The iron-porphyrin nitrosyl was synthesized by literature methods [27]. The Fe(TPP)(NO)⁻ complex was generated by borohydride reduction.

2.2. Instrumentation

RRDE and voltammetric procedures have been described previously [28]. Spectroelectrochemical experiments used a low-volume thin layer quartzglass cell purchased from BAS Inc. A platinum mesh was used as the working electrode and a platinum wire was used as the auxiliary electrode. Potentials were measured relative to the Ag/AgNO₃ (in CH₃CN) reference electrode. The UV-visible spectra were recorded on a HP 8452A diode array spectrophotometer. All solutions were prepared in the glovebox and sealed with Teflon tape. UV-visible spectroelectrochemical experiments were carried out by stepping to potentials sufficiently negative to ensure complete electrolysis. The resonance Raman spectra were measured at 77 K with 406.7 nm excitation, with a total collection time for each spectrum of 40 min. The power level was 1.0 mW and the slit 15 μm.

2.3. Computational Methods

Evolving Factor Analysis was carried out using MATLAB and PLS_Toolbox (Eigenvector Research, Inc.). The RRDE derivative data were fitted and smoothed with MATLAB using a Savitzky-Golay 7 point method.

3. Results and discussion

3.1. Cyclic voltammetry of Fe(TPP)(NO)

The cyclic voltammetry of Fe(TPP)(NO) in THF/0.10 M TBAP is shown in Fig. 1. A reversible wave was observed with an E° of -1.238 ± 0.003 V. The wave was broader than a reversible wave ($\Delta E_p = 85 \pm 4$ mV) due to the solution resistance of THF. With the addition of 20% (by volume) of the aprotic RTIL, EDPAmNTf₂ (EDPAm⁺ = ethyldimethylpropylammonium, NTf₂⁻ = bis-(trifluoromethylsulfonyl)imide), the wave was shifted to more positive potentials ($E^\circ = -1.143 \pm 0.003$ V), and the peak current decreased. The decrease in the peak current was due to the increased viscosity of the THF/AmNTf₂ mixture. The wave remained reversible in the mixture, indicating that the nitroxyl product, Fe(TPP)(NO)⁻, was stable in the presence of the RTIL, and that the transfer in/out of the RTIL nanodomain was fast compared to the cyclic voltammetric time scale. This was consistent with previous work [14,23,24]. The shift of 95 ± 4 mV in 20% EDPAmNTf₂ was larger than the observed shift for Fe(FP)^{0/-} (41 mV) (FP = tetrakis(pentafluorotetraphenyl)porphyrin) [25], or Ni(OEP)^{0/-} (71 mV) in the same mixture [23]. The shift in potential for Fe(TPP)(NO) was similar to that observed for Ni(OEPone)^{0/-}, where infrared spectroscopy showed a strong interaction between the carbonyl on the porphyrin ring and the RTIL nanodomain [23]. In both these examples (Fe(TPP)(NO)⁻ and Ni(OEPone)^{0/-}), there is an oxygen atom peripheral to the complex which contained a strong negative charge. For the other examples, the charge was more diffuse, and the shifts were smaller.

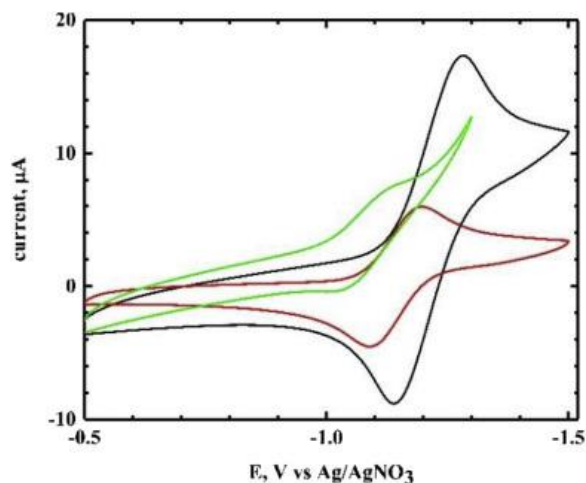
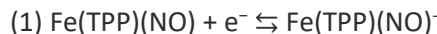


Fig. 1. Cyclic voltammetry of 4 mM Fe(TPP)(NO) in THF. Black trace: THF; Red trace: THF/20% EDPAmNTf₂; green trace: THF/20% EDPAmNTf₂/2% HAmOTf. Scan rate = 100 mV/s. Electrolyte: 0.10 M TBAP. Working electrode: platinum.

When 2% of the protic diethylmethylammonium triflate (HAmOTf) was added to the solution, the wave became much less reversible (Fig. 1). An additional shift in the peak potential was observed (E_{pf} shifted from -1.197 V to -1.156 V, both values ± 3 mV). This additional shift of 41 ± 4 mV was significant considering that the total RTIL concentration only increased from 20% to 22%. This indicates that the protic RTIL interacted more strongly with the iron-nitroxyl than the aprotic RTIL. The shift in potential and the decrease in the current for the reverse wave has been observed for Fe(OEP)(NO) [11] and is consistent with a strong interaction between the acid and the nitroxyl product.



3.2. Visible spectroelectrochemistry of Fe(TPP)(NO)

In order to identify the chemical species formed, the reduction product, Fe(TPP)(NO)⁻, was generated using visible spectroelectrochemistry. The visible spectroelectrochemistry of Fe(TPP)(NO) in THF is shown in Fig. S1. The THF spectrum was consistent with previous work [29]. The experiment was repeated in THF/20% EDPAmNTf₂ (Fig. 2A). The visible spectroelectrochemistry of Fe(TPP)(NO) in the presence and absence of EDPAmTf₂ was quite similar. The most significant difference was in the Soret region which shifted by 1 nm in the absence of EDPAmNTf₂, but was red-shifted from 412 to 416 nm in the presence of that RTIL, which indicated a significant interaction between the RTIL and Fe(TPP)(NO)⁻.

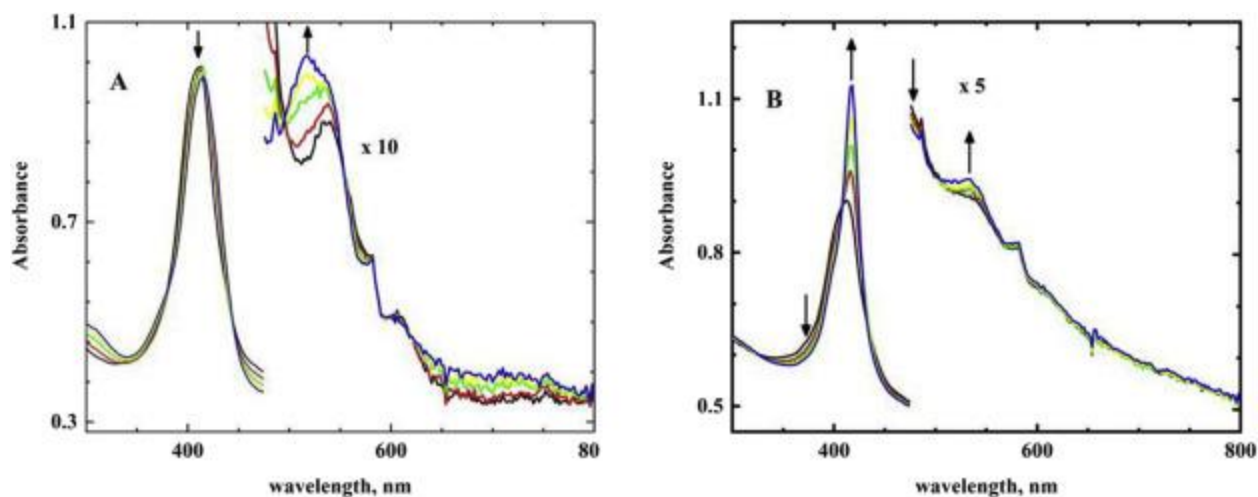


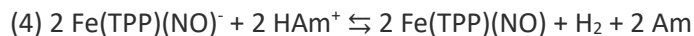
Fig. 2. Spectroelectrochemistry of Fe(TPP)(NO). A. Fe(TPP)(NO) in THF with 20% EDPAmTf₂. Time: 0 s (black), 25 s (red), 70 s (green), 121 s (yellow) and 186 s (blue). B. Fe(TPP)(NO) in THF/0.20% HAmOTf at -1.2 V. Time: 0 s (black), 20 s (red), 40 s (green), 100 s (yellow) and 200 s (blue).

The spectroelectrochemistry of the Fe(TPP)(NO) in the presence of HAmOTf is shown in Fig. 2B. The results were significantly different from what was observed in the absence of HAmOTf, but were similar to the changes observed for the reduction of Fe(OEP)(NO) in weak acids [11,30]. The strong Soret band at 416 nm was indicative of a low spin ferrous complex, which has been identified as a hydroxylamine complex. Evolving Factor Analysis (EFA) [14,31,32] of Fig. 2B was carried out, and the results are shown in Fig. S2. This result clearly showed the presence of three factors, which based on previous work [11,30], can be identified as Fe(TPP)(NO), Fe(TPP)(HNO) and Fe(TPP)(H₂NOH). In voltammetry, the reduction of Fe(TPP)(HNO) to Fe(TPP)(H₂NOH) occurs in a second wave due to the sluggishness of the multi-electron reduction. In spectroelectrochemistry, the longer time scale allows the two waves to overlap and it is difficult to stop the reduction at one-electron [11]. Further reduction of the iron-HNO complex to iron-H₂NOH can be prevented by restricting the number of reducing equivalents [11].

The visible spectrum of the intermediate, Fe(TPP)(HNO), was generated by the reduction of Fe(TPP)(NO) to Fe(TPP)(NO)⁻, followed by the addition of 0.5% HAm⁺ (Fig. S3). The Soret band was blue-shifted and the spectrum was quite similar to Fe(TPP)(NO). The first impression was that the Fe(TPP)(NO)⁻ complex had been oxidized back to Fe(TPP)(NO) with the release of H₂, a known reaction with stronger acids [10,29]. But recent work by Rahman and Ryan [11] showed that the Fe(OEP)(HNO) complex has a spectrum quite similar to Fe(OEP)(NO), but was a chemically distinct species. To verify that the iron-nitroxyl species was still present after the addition of the RTIL, resonance Raman spectroscopy of Fe(OEP)(NO) and its reduced species was carried out.

3.3. Resonance Raman spectroscopy

As was pointed out in the UV/visible spectroelectrochemistry section, there were only minor differences in the visible spectra of Fe(TPP)(NO) and Fe(TPP)(NO)⁻ with HAmOTf. The addition of a weak acid might protonate Fe(TPP)(NO)⁻, or the iron-nitroxyl might react with the weak acid to regenerate Fe(TPP)(NO) and H₂ ((3), (4)).



The resonance Raman spectra of Fe(TPP)(NO), Fe(TPP)(NO)⁻ and Fe(TPP)(NO)⁻ with 0.50% HAmOTf are shown in Fig. 3. The ν_{NO} band for Fe(TPP)(NO) can be clearly seen in Fig. 3 at 1673 cm⁻¹ which shifted to

1625 cm^{-1} upon substitution of ^{na}NO with ^{15}NO (na = natural abundance) (difference spectrum is trace A of Fig. 3). After chemical reduction to form $\text{Fe}(\text{TPP})(\text{NO})^-$ (visible spectrum in Fig. S4), the band at 1673 cm^{-1} in the resonance Raman spectrum disappeared (Fig. 3). The ν_{NO} for the nitroxyl is weak and could not be unambiguously identified in this spectrum. Upon addition of HAmOTf, the vibration at 1673 cm^{-1} did not reappear. These results clearly showed that Reaction (4) was not occurring, and the visible spectrum for $\text{Fe}(\text{TPP})(\text{NO})^-$ with HAmOTf (Fig. S4, green trace) was not $\text{Fe}(\text{TPP})(\text{NO})$.

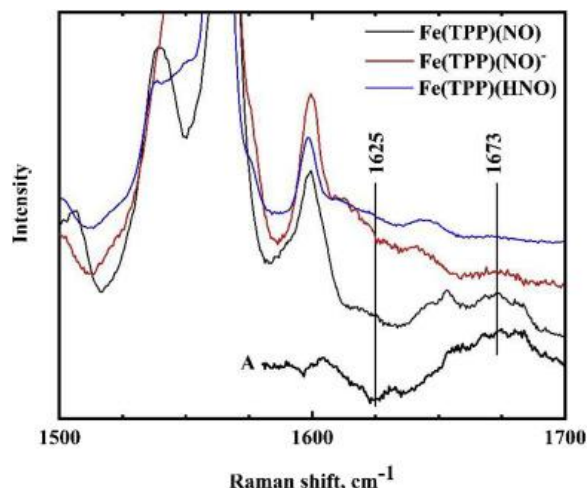


Fig. 3. Resonance Raman spectra of $\text{Fe}(\text{TPP})(\text{NO})$ and $\text{Fe}(\text{TPP})(\text{NO})^-$ in the absence and presence of 0.50% HAmOTf ($\text{Fe}(\text{TPP})(\text{HNO})$). A $\text{Fe}(\text{TPP})(^{na}\text{NO})-\text{Fe}(\text{TPP})(^{15}\text{NO})$.

In order to investigate the voltammetry in more detail, rotating ring disk electrode (RRDE) voltammetry was used. The advantage of this technique is that current measurements are carried out on the limiting current plateau and the kinetic analysis is not affected by electron transfer parameters such as k° and α . The measure for the stability of the product formed is the collection efficiency, N_k , which is the ratio of the absolute values of the ring current to the disk current.

3.4. RRDE voltammetry of $\text{Fe}(\text{TPP})(\text{NO})$

The RRDE voltammetry of $\text{Fe}(\text{TPP})(\text{NO})$ in THF is shown in Fig. 4A (black trace). In RRDE voltammetry (a brief description of RRDE voltammetry is given in the Supporting Information), the current at the ring and disk has a sigmoidal shape. The current at the ring will mirror the disk current with an opposite sign.

$$(5) i_R = -N_k \cdot i_D$$

where i_D and i_R are the ring and disk currents, respectively. If the reduction product is stable, N_k will be given by the geometry of the electrode, and will be constant as the rotation rate is changed. If the reduction product is unstable, N_k will decrease and its theoretical value can be calculated in many cases by the use of digital simulation [28,33]. The derivative of the disk or ring current will have a peak shape, and is given by Eq. (6):

$$(6) \frac{di}{dE} = \frac{i_L \exp((E-E^\circ)/S)}{S(1+\exp((E-E^\circ)/S))^2}$$

where $S = RT/F$ for a reversible system, and $R =$ gas constant, $T =$ temperature in K and F is Faraday's constant. In practice, the value of S may be larger than the theoretical value due to uncompensated resistance and/or slow electron transfer.

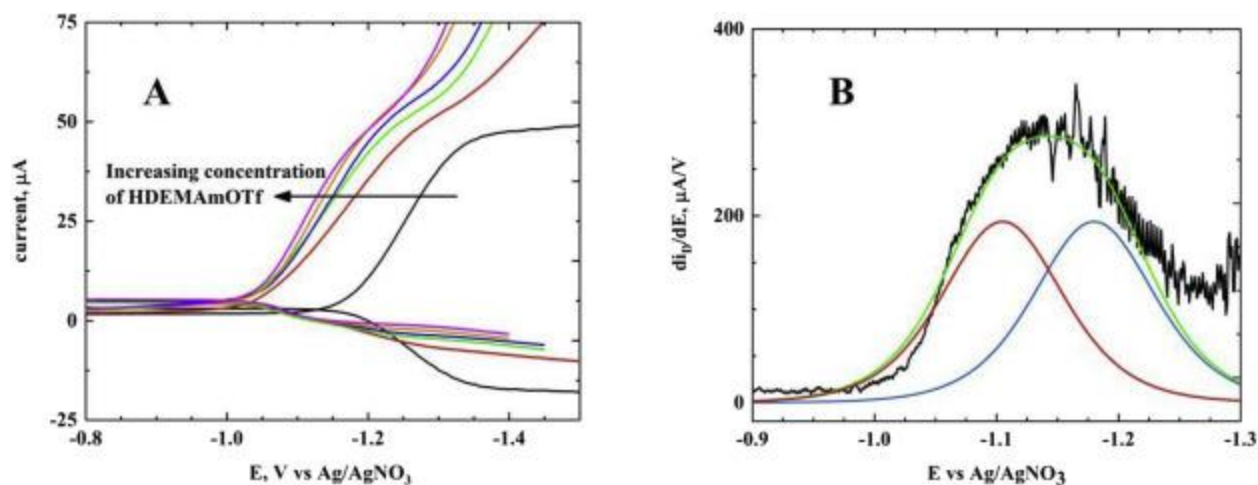


Fig. 4. A. RRDE of Fe(TPP)(NO) in THF. Concentration of HAMOTf: 0% (black), 0.10% (red), 0.25% (green), 0.50% (blue), 1.5% (orange), 4.5% (magenta). Rotation rate: 200 rpm. Ring/disk: platinum. B. Derivative of the disk current at 0.50% and 200 rpm. Black: experimental derivative current, Green: calculated derivative current, Blue: derivative current for wave at $E_{1/2,1}$. Red: derivative current for wave at $E_{1/2,2}$.

The derivation of Eq. (6) is given in the Supplemental Information. In the absence of the RTIL, the reduction product, Fe(TPP)(NO)⁻, in Reaction (1) was stable with a collection efficiency corresponding to a chemically reversible system (Table S1). When HAMOTf was added to the solution, the wave shifted to more positive potentials (Fig. 3A), but the limiting disk current was unchanged, indicating that the reduction was still one-electron, and that Fe(TPP)(HNO) did not disproportionate under RRDE conditions (this would have led to an EC catalytic wave and an increase in the limiting disk current). This shift indicated that there was a strong interaction between the Fe(TPP)(NO)⁻ species and the acidic cation, HAM⁺. A close examination of Fig. 3A also shows other important features. Not only was the wave shifted with the addition of HAMOTf, but it was significantly broader (slope of the log(i_{L-1})/ i) plots in the rising part of the wave. As the amount of HAMOTf was increased, the wave became sharper but the E° shifts were not as large. Fig. 4B shows the derivative of the disk current from Fig. 4A with the addition of 0.25% RTIL. The derivative was broader than expected from Eq. (6). It was possible to deconvolute the wave into two waves of roughly equal heights using Eq. (6) for two redox processes with different E° values (see Supporting Information for details). The E° values were calculated from the best-fit of the sum of the derivatives (Eq. (S6)). The residuals between the experimental and calculated derivative of the currents are shown in Fig. S5. For most of the wave, the deviations were small. Initially (see Fig. 4B/S5), the experimental derivative of the current did not rise as fast as the model, and, at the end of the scan, the second wave (reduction of Fe(TPP)(NO)⁻ to Fe(TPP)(H₂NOH)) began to overlap the first wave. The initial deviations may be due to kinetic features involving the RTIL nanodomains that are not in the model, and will be discussed further when the ring current is examined.

This process was repeated with the remaining waves for the mixtures (Fig. S6). By this procedure, it was possible to determine the two E° values (Table S2). The dependence of the two E° values on the %RTIL had significantly different concentration dependencies. The more positive E° (E°_2) was essentially independent of the %RTIL, while the second wave (E°_1) shifted significantly with %RTIL (Fig. 5). The more positive wave, E°_2 , was consistent with the incorporation/reaction of Fe(TPP)(NO)⁻ within the RTIL nanodomain (Reaction (7)).



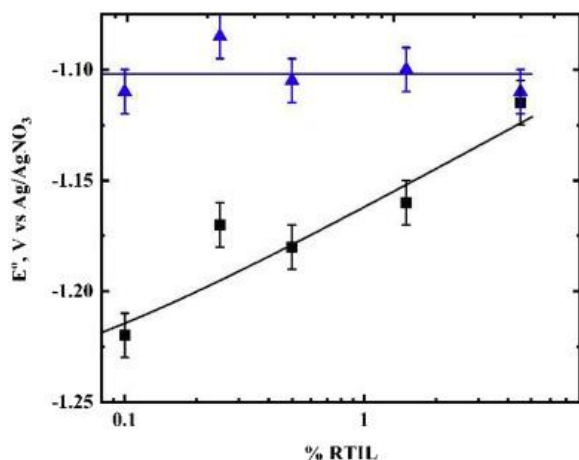


Fig. 5. Variation in the E°_1 and E°_2 values for Fe(TPP)(NO) with the %HAMOTf. Black line/symbols: E°_1 ; blue line/symbols: E°_2 .

In the RTIL nanodomain, the RTIL will encompass the substrate, and E°_1 (Reaction (7)) will be relatively independent of the %RTIL, as the reduced species would see a constant concentration of the protic species (given by the RTIL density).

The E°_1 values reflect interactions within the THF domain ((8), (9)).



where K is the equilibrium constant for Reaction (9). Within the THF domain, the equilibrium for Reaction 9 will depend upon the concentration of HAM^+ . Using this model, the black line in Fig. 5 was drawn with a K value of 20 for Reaction (9).

The effect of the protic RTIL on the redox potential was quite dramatic when compared to other weak acids. The acid, HAM^+ , which has a pK_a of about 10.8 (based on triethylammonium), is a weaker acid than phenol ($\text{pK}_a = 10.0$). The reduction of Fe(TPP)(NO) in THF with phenol has been previously studied [34]. In the range of phenol concentrations between 10 and 500 mM, the E° value shifted less than 10 mV, indicating a weak interaction between Fe(TPP)(NO) $^-$ and phenol. In this case, 0.1% (6 mM) RTIL caused a shift of 182 ± 4 mV. This value was even larger than the shift caused by the aprotic RTIL. Clearly, interactions stronger than ion-pairing were involved.

The collection efficiency is a measure of the stability of the redox product (Fe(TPP)(NO) $^-$). When Fe(TPP)(NO) $^-$ reacts with an acid such as HAMOTf, the collection efficiency will decrease. The currents in RRDE are steady-state currents, and the time parameter is controlled by the rotation rate, ω . The larger the rotation rate, the shorter the transit time for Fe(TPP)(NO) $^-$ between the disk and the ring, and the less time that it has to react. The values of N_k as a function of ω and %RTIL are shown in Table S1. For all rotation rates, the collection efficiencies decreased as %RTIL increased. This indicated that the rate of formation of the Fe(TPP)(HNO) complex was dependent upon the concentration of the protic RTIL. For an irreversible reaction, N_k should also decrease as ω was decreased (more time for the reaction to occur). This did not occur in this case (Table S1). This case has been examined recently in detail, and this behavior (N_k increasing as ω decreased) was evidence that Reaction 2 was reversible [28,35]. This is due to the additional time for the reverse reaction (oxidation of Fe(TPP)(HNO) to Fe(TPP)(NO) to occur). This can be clearly seen in Table S1 where N_k decreased as ω increased. Quantitative analysis of Table S1 is limited because the presence of RTIL nanodomains makes the analysis more complex, as the rate of the back reaction for Reaction (2) may be different between the RTIL (Reaction (7)) and

THF (Reaction (9)) nanodomains. This can be seen for the highest RTIL concentration where the N_k values are relatively constant with ω .

The question remains whether $\text{Fe}(\text{TPP})(\text{NO})$ was initially in the RTIL domain or whether it was reduced and then transferred to the RTIL domain. To investigate this, the rotation rate was varied for the 0.50% HAm^+ mixture. The derivative of the disk current is shown in Fig. 6. The results show that (8), (9) dominate over Reaction (7) as the rotation rate is increased. This can be seen by the rise in the derivative current at about -1.2 V at higher rotation rates (current due to the wave at $E_{1/2,1}$).

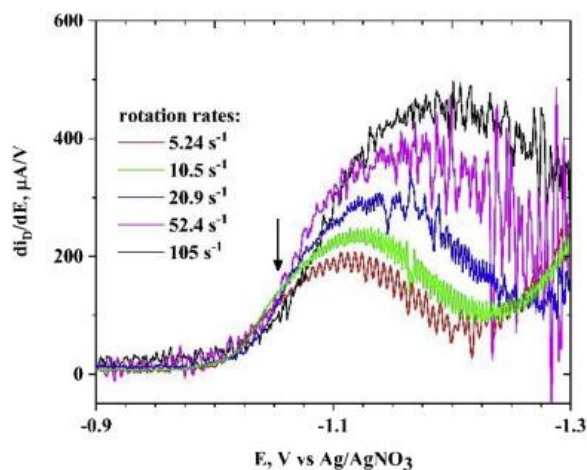


Fig. 6. Derivative disk current for the reduction of $\text{Fe}(\text{TPP})(\text{NO})$ in THF and 0.50% HAmOTf as a function of rotation rate.

Fig. 6 showed two regions, with different relationships between the current and the rotation rate. In the region to the left of the black arrow, the current (and derivative) was independent of rotation rate, indicating that this current was not controlled by diffusion. To the right of the arrow, the current depended upon rotation rate, showing that this region was controlled by diffusion. The limiting current was proportional to the square root of rotation rate (diffusion controlled). The region with little dependence on rotation rate indicated that there was a rate limiting step controlling the reduction process [36,37]. In this case, it may be due to saturation of the RTIL nanodomain near the electrode. This was also the region where there was deviation between the experimental and calculated derivative of the disk currents (Fig. 4B). As the %RTIL increased, more $\text{Fe}(\text{TPP})(\text{NO})$ was reduced at the more positive wave, which was consistent with the incorporation of $\text{Fe}(\text{TPP})(\text{NO})^-$ into the RTIL nanodomain, as the number of nanodomain particles increased (Fig. S6). The more positive wave (Reaction (7)) became more important as %RTIL increased, but the rising part of the wave shifted very little as the potential was determined by the RTIL nanodomain not its concentration. It is interesting that nanodomains were formed at very low concentrations of the RTIL.

Further evidence for the two reduction pathways can be seen in the ring currents (Fig. 4A). The derivative of the ring currents is shown in Fig. 7. The ring currents also showed two oxidation peaks in the derivative. The more positive peak is due to the oxidation of $\text{Fe}(\text{TPP})(\text{HNO})$ from the RTIL domain, while the more negative peak is due to the oxidation of $\text{Fe}(\text{TPP})(\text{NO})^-$ from the THF domain. The additional time between the reduction at the disk and the oxidation at the ring allowed for more of the $\text{Fe}(\text{TPP})(\text{NO})^-$ to be incorporated into the RTIL nanodomain. A comparison of Fig. 4B, where roughly 50% of the current proceeds through incorporation in the RTIL nanodomain with Fig. 7, showed that close to 2/3 of the oxidation at the ring is due to the RTIL nanodomain. These proportions should be considered estimates as oxidation/reduction will shift the equilibrium between the two domains. The substantial current at the ring also provides strong evidence that the visible spectrum for $\text{Fe}(\text{TPP})(\text{NO})^-$ in the presence of HAmOTf is not due to the disproportionation to form $\text{Fe}(\text{TPP})(\text{NO})$ and H_2 . If this

were to occur, the ring oxidation current should have disappeared as the concentration of HAmOTf increased (and the disk currents should have increased).

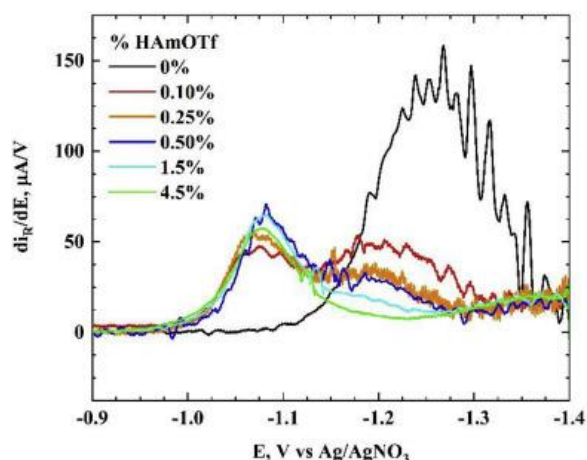


Fig. 7. Derivative of the ring current for Fe(TPP)(NO) in THF as a function of %HAmOTf at a rotation rate of 20.9 s^{-1} .

4. Conclusions

A protic ionic liquid has been shown to cause significant shifts in the reduction potential, well beyond the values expected based on ion-pairing or the cation pK_a . This should make them particularly attractive for catalysis. The nanostructure of the RTIL can force the cation and substrate anion to be correctly oriented for reduction, which will facilitate the reduction process. This has an advantage over molecular acids where high concentrations of phenol are needed to protonate and reduce Fe(TPP)(NO) to Fe(TPP)(NH₂OH). These results show that the reaction in the protic RTIL occurred at much lower acid concentrations than observed with molecular acids and was subsequently efficiently reduced by a multi-electron process to Fe(TPP)(NH₂OH). This was probably driven by the high local proton concentration in the RTIL nanodomain (HAm⁺) which can accelerate the reduction process.

For aprotic RTIL/molecular solvent mixtures, the redox process usually remained chemically reversible over the range of mixture concentrations [14,[23], [24], [25]]. The primary effect was shifting the reduction potential to more positive potentials. With protic RTILs, the RTIL itself became a reactive species rather than a media for neutralizing a charged species. This reactivity can be observed with RRDE voltammetry where the low collection efficiency for the Fe(TPP)(NO)/Fe(TPP)(NO)⁻ reduction indicated that there was a strong interaction between the substrate and the RTIL nanodomains. Changes in the visible spectrum were not due to the RTIL environment alone as minimal changes were observed for aprotic RTIL/molecular solvent mixtures. These spectral changes for the reduced species were dramatic even at low concentrations of the protic RTIL. The nature of the Fe(TPP)(HNO) complex is not entirely clear. Further studies are in progress in our laboratory to further characterize this complex.

Acknowledgement

The authors would like to thank James Kincaid for the use of his resonance Raman equipment.

Appendix A. Supplementary data

The following is the supplementary data to this article:

[Download Acrobat PDF file \(963KB\)](#)[Help with pdf files](#)

Supporting Information.

Research data for this article

for download under the CC BY NC 3.0 licence

Data for: Proton-Coupled Reduction of an Iron Nitrosyl Porphyrin in the Protic Ionic Liquid Nanodomain
Original voltammetric and spectroelectrochemical data for the reaction of a protic RTIL with Fe(TPP)(NO) nitroxyl

Dataset

489KB

FeNO RTIL data.xlsx

[View dataset on Mendeley Data](#)

[About research data](#)

References

- [1] O. Einsle, A. Messerschmidt, R. Huber, P.M.H. Kroneck, F. Neese. **Mechanism of the six-electron reduction of nitrite to ammonia by cytochrome c nitrite reductase.** *J. Am. Chem. Soc.*, 124 (2002), pp. 11737-11745
- [2] D. Bykov, F. Neese. **Six-electron reduction of nitrite to ammonia by cytochrome c nitrite reductase: insights from density functional theory studies.** *Inorg. Chem.*, 54 (2015), pp. 9303-9316
- [3] A. Daiber, H. Shoun, V. Ullrich. **Nitric oxide reductase (P450_{nor}) from *Fusarium oxysporum*.** *J. Inorg. Biochem.*, 99 (2005), pp. 185-193
- [4] B.A. Averill. **Dissimilatory nitrite and nitric oxide reductases.** *Chem. Rev.*, 96 (1996), pp. 2951-2964
- [5] M.Z. Cabail, J. Kostera, A.A. Pacheco. **Laser photoinitiated nitrosylation of 3-electron reduced nm europaea hydroxylamine oxidoreductase: kinetic and thermodynamic properties of the nitrosylated enzyme.** *Inorg. Chem.*, 44 (2005), pp. 225-231
- [6] F. Doctorovich, D. Bikiel, J. Pellegrino, S.A. Suárez, A. Larsen, M.A. Martí. **Nitroxyl (azanone) trapping by metalloporphyrins.** *Coord. Chem. Rev.*, 255 (2011), pp. 2764-2784
- [7] C. Riplinger, F. Neese. **The reaction mechanism of cytochrome P450 NO reductase: a detailed quantum mechanics/molecular mechanics study.** *ChemPhysChem*, 12 (2011), pp. 3192-3203
- [8] A.A.A. Attia, R. Silaghi-Dumitrescu. **Computational investigation of the initial two-electron, two-proton steps in the reaction mechanism of hydroxylamine oxidoreductase.** *J. Phys. Chem. B*, 118 (2014), pp. 12140-12145
- [9] E.G. Abucayon, R.L. Khade, D.R. Powell, Y. Zhang, G.B. Richter-Addo. **Hydride attack on a coordinated ferric nitrosyl: experimental and DFT evidence for the formation of a heme model-HNO derivative.** *J. Am. Chem. Soc.*, 138 (2016), pp. 104-107
- [10] L.E. Goodrich, S. Roy, E.E. Alp, J. Zhao, M.Y. Hu, N. Lehnert. **Electronic structure and biologically relevant reactivity of low-spin {FeNO}⁸ porphyrin model complexes: new insight from a bis-picket fence porphyrin.** *Inorg. Chem.*, 52 (2013), pp. 7766-7780
- [11] M.H. Rahman, M.D. Ryan. **Redox and spectroscopic properties of iron porphyrin nitroxyl in the presence of weak acids.** *Inorg. Chem.*, 56 (2017), pp. 3302-3309
- [12] B.A. Rosen, A. Salehi-Khojin, M.R. Thorson, W. Zhu, D.T. Whipple, P.J.A. Kenis, R.I. Masel. **Ionic liquid-mediated selective conversion of CO₂ to CO at low overpotentials.** *Science*, 334 (2011), pp. 643-644
- [13] A. Atifi, D.W. Boyce, J.L. DiMeglio, J. Rosenthal. **Directing the outcome of CO₂ reduction at bismuth cathodes using varied ionic liquid promoters.** *ACS Catal.*, 8 (2018), pp. 2857-2863
- [14] A. Atifi, M.D. Ryan. **Electrochemistry and spectroelectrochemistry of 1,4-dinitrobenzene in acetonitrile and room temperature ionic liquids: ion pairing effects in mixed solvents.** *Anal. Chem.*, 86 (2014), pp. 6617-6625
- [15] A.J. Fry. **Strong ion-pairing effects in a room temperature ionic liquid.** *J. Electroanal. Chem.*, 546 (2003), pp. 35-39
- [16] K. Shimizu, M.F. Costa Gomes, A.A.H. Pádua, L.P.N. Rebelo, J.N. Canongia Lopes. **Three commentaries on the nano-segregated structure of ionic liquids.** *J. Mol. Struct.*, 946 (2010), pp. 70-76

- [17] C.S. Consorti, P.A.Z. Suarez, R.F. de Souza, R.A. Burrow, D.H. Farrar, A.J. Lough, W. Loh, L.H.M. Da Silva, J. Dupont. **Identification of 1,3-dialkylimidazolium salt supramolecular aggregates in solution.** J. Phys. Chem. B, 109 (2005), pp. 4341-4349
- [18] A.A.H. Pádua, M.F. Costa Gomes, J.N.A. Canongia Lopes. **Molecular solutes in ionic liquids: a structural perspective** Acc. Chem. Res., 40 (2007), pp. 1087-1096
- [19] D.R. Schreiber, M.C. De Lima, K.S. Pitzer. **Electrical conductivity, viscosity, and density of a two-component ionic system at its critical point.** J. Phys. Chem., 91 (1987), pp. 4087-4091
- [20] I.C.M. Vaz, A. Bhattacharjee, M.A.A. Rocha, J.A.P. Coutinho, M. Bastos, L.M.N.B.F. Santos. **Alcohols as molecular probes in ionic liquids: evidence for nanostructuring.** Phys. Chem. Chem. Phys., 18 (2016), pp. 19267-19275
- [21] N.T. Scharf, A. Stark, M.M. Hoffmann. **Ion pairing and dynamics of the ionic liquid 1-Hexyl-3-methylimidazolium bis(trifluoromethylsulfonyl)amide ([C₆mim][NTf₂]) in the low dielectric solvent chloroform.** J. Phys. Chem. B, 116 (2012), pp. 11488-11497
- [22] J.D. Tubbs, M.M. Hoffmann. **Ion-pair formation of the ionic liquid 1-ethyl-3-methylimidazolium bis(triflyl)imide in low dielectric media.** J. Solut. Chem., 33 (2004), pp. 381-394
- [23] A. Atifi, M.D. Ryan. **Spectroscopic evidence of nanodomains in THF/RTIL mixtures: spectroelectrochemical and voltammetric study of nickel porphyrins.** Anal. Chem., 87 (2015), pp. 12245-12253
- [24] A. Atifi, M.D. Ryan. **Influence of RTIL nanodomains on the voltammetry and spectroelectrochemistry of fullerene C₆₀ in benzonitrile/room temperature ionic liquids mixtures.** Electrochim. Acta, 191 (2016), pp. 567-576
- [25] A. Atifi, M.D. Ryan. **Altering the coordination of iron porphyrins by ionic liquid nanodomains in mixed solvent systems.** Chem. Eur J., 23 (2017), pp. 13076-13086
- [26] M. Schmeisser, R. van Eldik. **Thermodynamic and kinetic studies on reactions of FeIII(meso-[tetra(3-sulfonatomesityl)porphin]) with NO in an ionic liquid. Trace impurities can change the mechanism!** Inorg. Chem., 48 (2009), pp. 7466-7475
- [27] I.-K. Choi, Y.M. Liu, Z. Wei, M.D. Ryan. **Reactions of hydroxylamine with metal porphyrins.** Inorg. Chem., 36 (1997), pp. 3113-3118
- [28] M.H. Rahman, M.D. Ryan. **The use of RRDE voltammetry to study acid-base reactions in unbuffered solutions.** Electrochim. Acta, 281 (2018), pp. 17-23
- [29] I.-K. Choi, Y. Liu, D. Feng, K.J. Paeng, M.D. Ryan. **Electrochemical and spectroscopic studies of iron porphyrin nitrosyls and their reduction products.** Inorg. Chem., 30 (1991), pp. 1832-1839
- [30] M.H. Rahman, M.D. Ryan. **Insight into solvent coordination of an iron porphyrin hydroxylamine complex from ¹H NMR, FTIR and DFT evidence.** Eur. J. Inorg. Chem. (2018), pp. 1762-1765
- [31] A. Atifi, K. Czarnecki, H. Mountacer, M.D. Ryan. **In situ study of the photodegradation of carbofuran deposited on TiO₂ film under UV light, using ATR-FTIR coupled to HS-MCR-ALS.** Environ. Sci. Technol., 47 (2013), pp. 8650-8657
- [32] R.L. Keeseey, M.D. Ryan. **Use of evolutionary factor analysis in the spectroelectrochemistry of *Escherichia coli* sulfite reductase hemoprotein and a Mo/Fe/S cluster.** Anal. Chem., 71 (1999), pp. 1744-1752
- [33] K.B. Prater. **Digital simulation of the rotating ring-disk electrode.** J.S. Mattson, H.B. Mark Jr., H.C. MacDonald Jr. (Eds.), Electrochemistry: Calculations, Simulation, and Instrumentation, Marcel Dekker, New York(1972), pp. 219-240
- [34] Y.M. Liu, M.D. Ryan. **The electrochemical reduction of iron porphyrin nitrosyls in the presence of weak acids.** J. Electroanal. Chem., 368 (1994), pp. 209-219
- [35] W.J. Albery, S. Bruckenstein. **Ring-disk electrodes. VII. Homogeneous and heterogeneous kinetics.** Trans. Faraday Soc., 62 (1966), pp. 2596-2606
- [36] F. Opekar, P. Beran. **Rotating disk electrodes.** J. Electroanal. Chem., 69 (1976), pp. 1-105
- [37] F.C. Anson. **Kinetic behavior to be expected from outer-sphere redox catalysts confined within polymeric films on electrode surfaces.** J. Phys. Chem., 84 (1980), pp. 3336-3338